Green Chemistry

Towards cost-competitive middle distillate fuels from ethanol within a market-flexible biorefinery concept

Journal:	*Green Chemistry*
Manuscript ID	GC-ART-08-2021-002854.R1
Article Type:	Paper
Date Submitted by the Author:	28-Oct-2021
Complete List of Authors:	Zhang, Junyan; Oak Ridge National Laboratory, Manufacturing Science Division; University of Maryland at College Park, Chemical and biomolecular engineering Yoo, Eunji; Argonne National Laboratory Davison, Brian; Oak Ridge National Laboratory, Biosciences Division Liu, Dongxia; University of Maryland at College Park, department of Chemical and Biomolecular Engineering Schaidle, Joshua; National Renewable Energy Laboratory, Catalytic Carbon Transformation & Scale-up Center Tao, Ling; National Renewable Energy Laboratory Li, Zhenglong; Oak Ridge National Laboratory, Manufacturing Science Division

ARTICLE

Towards cost-competitive middle distillate fuels from ethanol within a market-flexible biorefinery concept

Received 00th January 20xx,
Accepted 00th January 20xx

DOI: 10.1039/x0xx00000x

Junyan Zhang[a,b], Eunji Yoo[c], Brian H. Davison[d], Dongxia Liu[b], Joshua A. Schaidle[e], Ling Tao[e*], Zhenglong Li[a*]

Ethanol to middle distillates (ETMD) is a promising pathway to produce sustainable liquid fuels to decarbonize the hard-to-electrify transportation sectors due to (1) the abundant sugar/starch and lignocellulosic biomass, (2) the existing deployment scale of fuel ethanol production (~29 billion gallons/year globally), and (3) emerging opportunities in C_{2+} alcohol synthesis from CO_2. Here we report a conceptual market-responsive biorefinery centered around a new ETMD pathway based on one-step ethanol to butene-rich olefins (ETO) over a Cu-Zn-Y/Beta catalyst. Specifically, this ethanol conversion pathway comprises one-step ETO, oligomerization, and hydrotreating. This ETO is distinct from that in the conventional ethanol-to-jet process which is based on two-step ethanol to ethylene and ethylene oligomerization to butenes. Butene-rich olefins can be shifted to butadiene-rich products by simply changing the reaction atmosphere from hydrogen to inert gas over the same ETO catalyst. Leveraging the experimental results, baseline techno-economic analysis (TEA) and sensitivity analysis indicate that the ethanol conversion cost is $0.60/gallon gasoline equivalent (GGE), with opportunities for further cost reduction via improving the liquid hydrocarbon yield and space velocities, and process optimization on balancing dewatering of ethanol feed prior to the ETO step. The minimum fuel selling price (MFSP) of liquid hydrocarbons derived from corn starch ethanol with butadiene as coproduct is $1.64/GGE, in the range that is cost competitive with petroleum kerosene-type jet fuel. Projected MFSP for cellulosic ethanol (corn stover) derived hydrocarbons is below $3.00/GGE and co-production of butadiene further reduces the MFSP to $1.70/GGE. The Well-to-Wake life-cycle analysis indicates that 85% greenhouse gas emission reduction can be achieved when using corn stover compared to petroleum reference and the associated carbon credits will provide significant economic incentives to favor the cellulosic ethanol-derived hydrocarbon fuels. This study demonstrates a low-cost pathway to middle distillate fuels leveraging existing ethanol infrastructure, where catalysis innovation drives the reduction of process complexity and flexible coproduction of a value-added chemical product.

[a.] *Manufacturing Science Division, Oak Ridge National Laboratory, Oak Ridge, TN 37830, USA. *E-mail: liz3@ornl.gov.*
[b.] *Department of Chemical and Biomolecular Engineering, University of Maryland, College Park, MD 20742, USA.*
[c.] *Energy Systems division, Argonne National Laboratory, Chicago, Lemont, IL 60439, USA.*
[d.] *Bioscience Division, Oak Ridge National Laboratory, Oak Ridge, TN 37830, USA.*
[e.] *Catalytic Carbon Transformation & Scale-up Center, National Renewable Energy Laboratory, Golden, CO 80401, USA. *E-mail: Ling.Tao@nrel.gov.*
Electronic Supplementary Information (ESI) available. See DOI: 10.1039/x0xx00000x

1. Introduction

Sustainable middle distillate (MD) production from either biomass or CO_2 is an attractive option to decarbonize the aviation, marine and heavy-duty trucking sectors. Among various challenges that limit the extensive deployment of sustainable MD, realizing economic viability remains the top priority. Lowering the feedstock cost, improving carbon conversion efficiency to increase the liquid fuel yield, and enhancing process and energy efficiency are all critical measures for lowering the minimum fuel selling price (MFSP)[1,2]. Another crucial strategy is to capitalize on revenues from coproducts[3], analogous to petroleum refining, where significant revenue is made from chemical products despite much less production volume compared to fuels. A common challenge for the coproduct strategy is the majority of the coproducts have limited market volume[4] and significant amounts of coproducts are generally needed to offset the fuel production cost, leading to rapid market saturation. Therefore, when developing a new conversion pathway, it is important to coproduce chemical products with large market volume to lower the fuel production cost besides improving carbon conversion efficiency and process and energy efficiencies.

Among various biomass conversion technologies, ethanol upgrading is a promising pathway to produce large quantities of middle distillate fuels due to the well-established ethanol market (~29.0 billion gallons globally in 2019)[5], emerging opportunities in ethanol synthesis from CO_2[6], and the ethanol "blend wall". In this work, we report a pathway for ethanol to middle distillate fuels via one-step ethanol to butene-rich olefins. We also provide the detailed techno-economic analysis (TEA) and life-cycle analysis (LCA) to assess the state of technology and identify critical research and development (R&D) opportunities to further improve the cost competitiveness and lower the life-cycle greenhouse gas (GHG) emissions.

A single-step ethanol conversion pathway over metal-modified zeolites has been under development to produce aromatic-rich hydrocarbon blendstock[7,8]. To produce paraffinic type middle distillates, ethanol conversion generally involves ethanol dehydration to ethylene, ethylene oligomerization to butene-rich olefins, followed by further oligomerization of butene-rich olefins and hydrotreating[9]. Two process steps are needed to convert ethanol to butene-rich olefins and the ethanol dehydration step requires significant energy inputs since it is an endothermic reaction. Recent R&D activities have focused on improving the efficiency for such pathway, particularly targeting direct conversion of ethanol to C_{3+} olefins (ETO)[10–13], thereby avoiding the ethanol dehydration step and reducing the capital and the operating expenses.

There are three major types of reaction pathways for direct ETO, including Brønsted acid zeolite catalyzed pathway with ethylene as the intermediate, metal oxide catalyzed pathway with acetone intermediate, and pathway with 1,3-butadiene (butadiene, BD) as the intermediate over transition metal modified oxides. Direct ETO over conventional Brønsted acid zeolites (e.g., H-ZSM-5) generates ethylene first via ethanol dehydration which then further oligomerizes and cracks to form C_{3+} olefins; however, the presence of strong Brønsted acid sites and zeolite shape selectivity lead to significant formation of aromatics and light paraffins, restricting the C_{3+} olefin yield to <50%[8,14]. Generally, this type of reaction produces a mixture of propene and butenes with propene as the major olefin product at high reaction temperatures, e.g., >673 K. Another direct ETO approach is to convert ethanol to propene and/or isobutene over oxide catalysts with proper acid-base properties, such as Y/ZrO_2 and $ZnZrO_x$, where the reactions are generally following ethanol dehydrogenation, oxidation, and ketonization to acetone, and followed by acetone conversion to either propene[15] or isobutene[16]. In both the acetone formation and acetone to isobutene reaction steps, CO_2 is generated as a side product due to C-C bond cleavage, limiting the theoretical maximum carbon yield to C_{3+} olefins (e.g., 69% theoretical carbon yield to isobutene from ethanol[16]). $ZnZrO_x$-based catalysts primarily generate isobutene while the other oxide materials (e.g., ZrO_2, Sc/In_2O_3) mainly produce propene. This approach is also usually operated at high reaction temperatures, e.g., 673-823 K. The third pathway is catalyzed by transition metal promoted oxide catalysts (e.g., $Ag/ZrO_2/SiO_2$), where ethanol is converted to butenes via dehydrogenation, aldol condensation, Meerwein-Ponndorf-Verley (MPV) reduction, dehydration to butadiene and followed by hydrogenation to 1-butene and 2-butenes[13]. $Ag/ZrO_2/SiO_2$ was reported to produce ~69% selectivity of butene-rich C_{3+} olefins at near-complete ethanol conversion under hydrogen reducing environment at 673 K; however, significant ethylene (~19% selectivity) was observed.

Further oligomerization of these C_{3+} olefins is generally carried out at lower reaction temperatures, e.g., ~413 K over Amberlyst 36 and 413-533 K over H-ZSM-5 and H-Beta catalysts[17]. Among these olefins, butenes have been studied as important olefin intermediates for synthesizing middle-distillate-range liquid transportation fuels[14,19] as they are generally more reactive during oligomerization over solid acid catalysts compared to other olefins[17,20]. Therefore, an ideal ETO catalyst would need to produce butene-rich C_{3+} olefins at high selectivities and lower reaction temperatures, so that the oligomerization can produce high yield of middle distillate fuels more efficiently, and the heat management duties can be minimized between ETO and oligomerization steps due to the reduced operation temperature difference. All these advancements can lead to significant cost reduction for the middle distillate fuel production.

Recently we reported a Lewis acid Cu-Zn-Y/Beta catalyst to catalyze the ethanol-to-butene reaction via ethanol dehydrogenation, aldol condensation to crotonaldehyde, and followed primarily by hydrogenation to butyraldehyde, and subsequent hydrogenation and dehydration reactions to form butenes (solid arrows, Scheme 1)[11]. Cu sites promote the hydrogenation of crotonaldehyde C=C bond to form butyraldehyde in the presence of hydrogen. This catalyst exhibits 88% selectivity to butene-rich C_{3+} olefins at ~100% ethanol conversion (623 K). However, ethanol to middle distillates based on direct ETO over this catalyst has not been

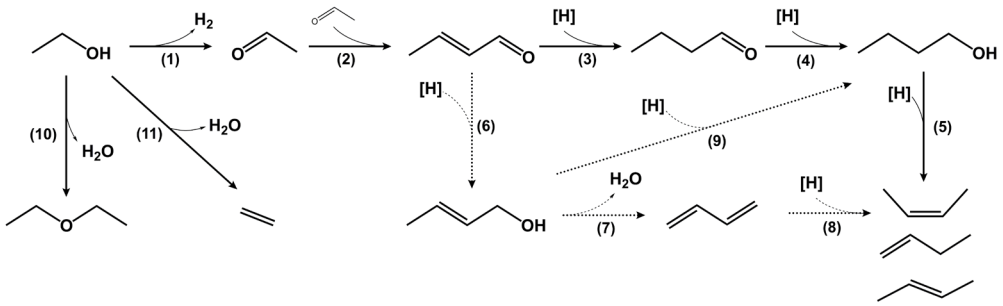

Scheme 1. Proposed reaction network of ethanol conversion to butenes. Solid arrows and dashed arrows indicate the primary and minor routes for ethanol to butenes, respectively. This scheme is adapted from Zhang et al.[11]

reported yet. Further, value-added coproduct opportunities have not been explored for neither this ETO route nor the other ETO pathways. The economic feasibility and life-cycle GHG emissions of this ethanol conversion pathway have to be investigated.

Here we report the impact of catalyst composition and reaction conditions on catalyst performance, which provides critical experimental inputs for process modeling, TEA and LCA. More importantly, we show that butadiene can be coproduced by simply changing the reaction carrier gas from hydrogen to inert gas over the same catalyst without modifying other reaction conditions. Butadiene is a value-added chemical coproduct with a large existing market[4] (>12 million MT/year[21]). Due to the feedstock shift from naphtha to shale gas for making ethylene, on-purpose butadiene production from renewable ethanol[22] can help to meet the rising demand of butadiene with the potential of reducing greenhouse gas emissions. Besides coproducing butadiene, the new ETO approach brings other benefits to the ethanol-to-middle-distillate technology by eliminating the endothermic ethanol dehydration step and reducing the number of unit operations in comparison with the ethylene-based process. Additionally, the demonstrated C_{3+} olefin selectivity exceeds that of the other direct ETO pathways by avoiding significant formation of CO_2 and light paraffins, leading to a higher liquid hydrocarbon yield and ultimately a lower MFSP.

This direct ETO was further configurated into a conceptual biorefinery design, which comprises biomass to ethanol via fermentation, ethanol separation, ETO, oligomerization and hydrotreating (Scheme 2). The downstream ethanol upgrading process is the focus and it can be operated as either an ethanol-to-middle-distillate mode (ETMD, no butadiene coproduct) or an ethanol-to-middle-distillate-and-butadiene (ETMDB) mode, where the latter mode can produce both liquid hydrocarbon fuels and butadiene and the ratio of butadiene:fuels can be adjusted by tuning the hydrogen partial pressure of the ETO step. The experimental results from the ETO and oligomerization steps were provided for techno-economic analysis (TEA) to evaluate the economic feasibility, and the major cost drivers were identified to provide guidance for further R&D activities. LCA was also performed to evaluate the life-cycle GHG emissions of this ethanol conversion pathway and guide further directions to reduce the carbon intensity. Market flexibility of this conceptual biorefinery was also discussed based on feedstock variability, production of different types of hydrocarbon fuels (jet and diesel), and generation of co-products.

2. Results and discussion

2.1 Ethanol to C_{3+} olefins and BD, and olefin oligomerization

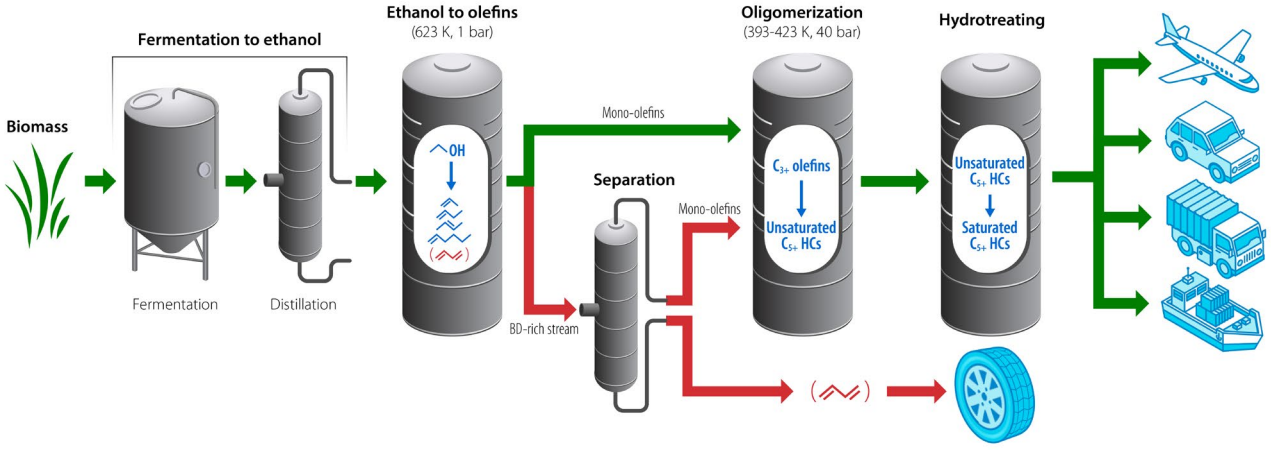

Scheme 2. Process scheme of a conceptual market-flexible biorefinery centered around ethanol to middle distillates. Green arrows indicate the ethanol-to-middle-distillate operation mode, while the red arrows show the ethanol-to-middle-distillate-and-butadiene operation mode. We considered either cellulosic biomass or corn starch as the biomass feedstock.

Table 1. Ethanol conversion and product selectivities over various catalysts at 603 K

Catalysts	Conv. %	Product selectivity (%)								
		Diethyl ether	Ethylene	Dehydration products	Acetal-dehyde	Butenes	BD	C_{3+} olefins	Dehydro-genation	Aldol condens-ation
DeAl-Beta	87	2.3	97	99	0.2	0.3	0	0.3	0.5	0.3
Cu/Beta	90	5.1	36	41	22	7.2	0	8.8	31	8.9
Zn/Beta	77	5.1	39	44	27	15	8.1	18	53	26
Cu-Y/Beta	89	4.5	9.0	13	14	49	0.1	71	85	71
Zn-Y/Beta	91	5.2	7.8	13	3.7	16	55	28	87	83
Cu-Zn-Y/Beta	89	3.3	10	13	9.6	59	0.8	75	85	76

Reaction conditions: 13.9 kPa ethanol, 94.3 kPa H_2, 603 K, WHSV = 0.62 h^{-1} for all the metal loaded catalysts, WHSV=0.93 h^{-1} for DeAl-Beta. Dehydration products consist diethyl ether and ethylene. Dehydrogenation products include acetaldehyde and all the C_{3+} hydrocarbons. Aldol condensation products contain all the C_{3+} hydrocarbons. C_{3+} olefins only contain mono-olefins. The relative errors in conversion and selectivities are ±5%.

2.1.1 Catalyst composition impact on ETO performance. Since this ETO reaction pathway involves acetaldehyde as the primary intermediate, Cu and Zn were selected to catalyze ethanol dehydrogenation[23,24]. To avoid significant CO_2 formation, aldol condensation of acetaldehyde is preferred over Lewis acid sites, such as Zr, Ti, or Y over siliceous zeolite supports[25]. Because of the trivalent nature and larger radius of Y^{3+}, it is considered as a softer Lewis acid[26], which makes a Y-based catalyst a promising option because it can catalyze acetaldehyde aldol condensation[24,10] while suppressing ethanol dehydration[27]. Further hydrogenation of C_4 aldehydes to alcohols could be catalyzed either via direct reduction with hydrogen over Cu sites[28] or through MPV reduction with an alcohol as a hydrogen donor over Lewis acid sites[24] (steps 3, 4, and 6, Scheme 1).

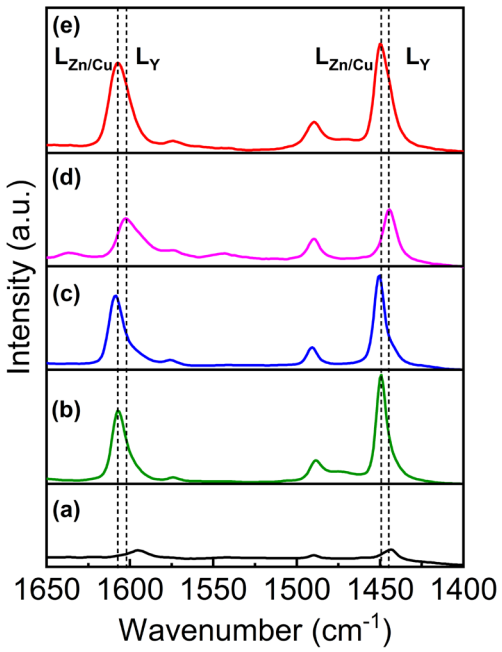

Figure 1. DRIFTS spectra collected on (a) DeAl-Beta, (b) Cu/Beta, (c) Zn/Beta, (d) Y/Beta, and (e) Cu-Zn-Y/Beta after pyridine saturation at 423 K.

Dealuminated zeolite Beta (DeAl-Beta) was selected as the support to anchor metal sites for all the catalysts used in this study because it is known for possessing a high density of silanol defects[29]. Monometallic (Cu/Beta and Zn/Beta), bimetallic (Cu-Y/Beta and Zn-Y/Beta) and trimetallic Cu-Zn-Y/Beta catalysts were further synthesized via a solid-state grinding approach with loadings of Cu, Zn and Y at ~1 wt.%, ~2 wt.% and ~7 wt.%, respectively. X-ray diffraction patterns and micropore volumes derived from N_2 adsorption isotherms for DeAl-Beta and metal loaded samples are consistent with the Beta topology as shown in Zhang et al[11]. Diffuse reflectance infrared Fourier transform spectroscopy (DRIFTS) measurements were performed on mono-, and trimetallic samples after pyridine saturation to probe the Lewis acid sites (Figure 1). Two peaks at 1450 and 1608 cm^{-1} are observed in the spectra of Cu/Beta and Zn/Beta, but absent from the DeAl-Beta spectra, indicating pyridine adsorption on Lewis acid Cu and Zn sites. Over Y/Beta, the presence of Lewis acid Y sites is indicated by the peaks centered around 1445 and 1603 cm^{-1} [10]. The trimetallic sample preserves the Lewis acid features shown in those monometallic samples, with the major peak at 1450 cm^{-1} and a shoulder at 1445 cm^{-1}. Other detailed characterizations of metal site distributions, oxidation states, and coordination environment were reported in Zhang et al[11].

DeAl-Beta primarily produces ethanol dehydration products at 603 K while Cu/Beta significantly promotes the dehydrogenation activity as reflected by the increase in dehydrogenation product selectivity from 0.5% to 31% at similar ethanol conversion in comparison with DeAl-Beta (Table 1). Similarly, Zn/Beta also exhibits 53% selectivity to dehydrogenation products. Y is further added to Cu/Beta or Zn/Beta to introduce Lewis acidity for promoting aldol condensation[10]. When comparing with Cu/Beta, Cu-Y/Beta demonstrates higher selectivity to aldol condensation products (71%) at similar ethanol conversion and butenes are the predominant products. Zn-Y/Beta also generates 83% selectivity of aldol condensation products; however, butadiene becomes the dominant coupling product. Adding Zn onto Cu-Y/Beta (Cu-Zn-Y/Beta) further enhances the selectivity of C_{3+}

olefins and aldol condensation products to 75% and 76%, respectively, in comparison with Cu-Y/Beta, particularly increasing butene selectivity (Table 1). Based on the fact that the trimetallic catalyst leads to high C_{3+} olefin selectivity, we chose to work with Cu-Zn-Y/Beta for the following studies. We would like to note the comparison of catalyst performance at high ethanol conversion is only to help understand why the trimetallic Cu-Zn-Y/Beta catalyst is selected for further optimizing reaction conditions. Strict comparisons of the catalyst activities and investigations of the catalytic functionalities of these metal sites are the focuses of another study[11].

2.1.2 ETO reaction condition optimization — experimental inputs for TEA. Ethanol conversion and C_{3+} olefin selectivity over Cu-Zn-Y/Beta were further optimized by varying the reaction temperature, weight hourly space velocity (WHSV), water concentration in the liquid feed, and hydrogen partial pressure. These experimental results were provided for TEA to allow more accurate predictions of the fuel production cost and to perform sensitivity analysis for understanding the process condition impact on the cost. Major cost drivers associated with the ETO catalyst and process will be identified to guide further catalyst and process development in section 2.2.

As shown in Figure 2, reaction temperatures were studied from 473 to 673 K to optimize catalyst performance while the other reaction conditions were kept constant (7.5 kPa ethanol, 99.3 kPa H_2, WHSV 0.52 h^{-1}). Ethanol conversion increases monotonically from 9.7% to 100% as the temperature was ramped up to 623 K, after which complete ethanol conversion remains. The C_{3+} olefin selectivity is optimized to 89% with 100% conversion at 623 K. Butene selectivity is less than C_{5+} olefin selectivity below 573 K, while butenes dominate the C_{3+} olefin stream above 573 K with maximum butene selectivity (61%) showing up at 623 K. At lower reaction temperatures (473-523 K), significant C_4 oxygenates (e.g., butyraldehyde, 1-butanol, crotyl alcohol) are observed, which are derived from the aldol condensation product (crotonaldehyde) after further hydrogenation reactions (steps 3, 4 and 6, Scheme 1). All of the C_4 oxygenates are completely consumed when the reaction temperature is above 573 K, leading to butene formation.

Residence time or space velocity is directly related to the reactor sizing and catalyst cost in the process design and TEA. As shown in Figure S1, ethanol conversion and product selectivities of C_{3+} olefins, butenes and C_{5+} olefins increase as residence time rises from 0.34 to 1.9 g_{cat} h g_{EtOH}^{-1}. Acetaldehyde continues to be consumed to make C_{3+} olefins as indicated by the decrease of acetaldehyde from 17% to 1.4% while the C_{3+} olefin selectivity increases from 47% to 89%. Negligible C_4 oxygenates are present even at very low residence time, indicating fast conversion of these C_4 intermediates to butenes at this temperature.

For this ETO reaction, water is produced in multiple steps, such as aldol condensation (step 2, Scheme 1) and dehydration of crotyl alcohol and 1-butanol (steps 5 and 7). Aqueous ethanol is also likely to be a favorable feed for ethanol conversion to save energy and capital expense in ethanol dewatering[8].

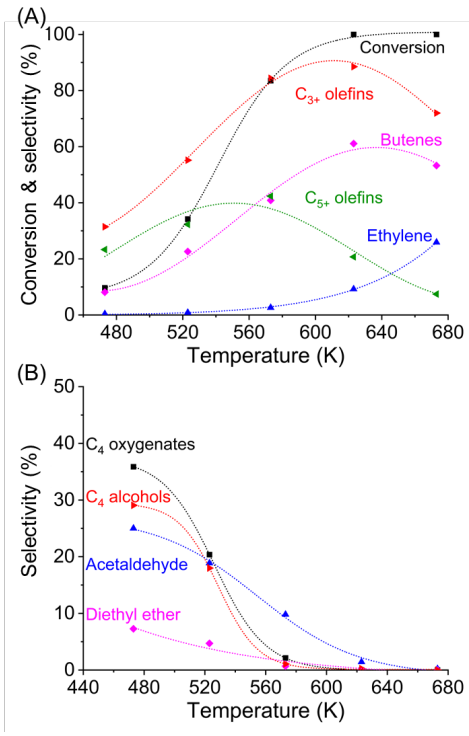

Figure 2. (A) Ethanol conversion and olefin selectivities; and (B) oxygenate selectivities over Cu-Zn-Y/Beta at different reaction temperatures. Reaction conditions: ~0.19 g Cu-Zn-Y/Beta catalyst diluted in 0.8 g SiC, 0.52 h^{-1} WHSV, 7.5 kPa ethanol, 99.3 kPa H_2. Data is collected at time on stream (TOS) 1.1 h. C_4 oxygenates include butyraldehyde, butanone, 1-butanol and crotyl alcohol. C_4 alcohols include 1-butanol and crotyl alcohol. Light alkanes are within 0-1.0% at all conditions. C_{5+} olefins include pentenes and hexenes.

Cofeeding water has been reported to inhibit the C-C bond formation for the ethanol-to-butanol Guerbet chemistry when ethanol reacts over the surfaces of hydroxyapatite (HAP) or MgO[30]. Therefore, it is critical to study the impact of water on the ETO reaction with our Cu-Zn-Y/Beta catalyst to allow the opportunity for feeding wet ethanol. Figure S2 shows the comparison of ethanol conversion and product selectivities with pure ethanol and aqueous ethanol with 13 wt.% of water (within the water concentration range of wet ethanol after rectification column during ethanol purification) while keeping ethanol and hydrogen partial pressure the same (623 K, 5.7 kPa ethanol, 79.6 kPa hydrogen balanced with Ar). When there is no co-fed water, the initial ethanol conversion is ~100% and the C_{3+} olefin selectivity is ~89% at 1.9 h TOS (Figure S2). No significant change of ethanol conversion is observed, with only a slight decrease in the C_{3+} olefin selectivity to 84%, after 12 h TOS. The major product is still butenes at a selectivity of ~65% during the 12 h TOS. When we cofed 13 wt.% water, both ethanol conversion and product selectivities are very similar to those with pure ethanol feed, suggesting 13 wt.% water does not have a significant impact on the catalyst performance. Although this could not ensure the long-term (e.g., >1000 h) steam stability of this catalyst, it provides good indication that this Cu-Zn-Y/Beta

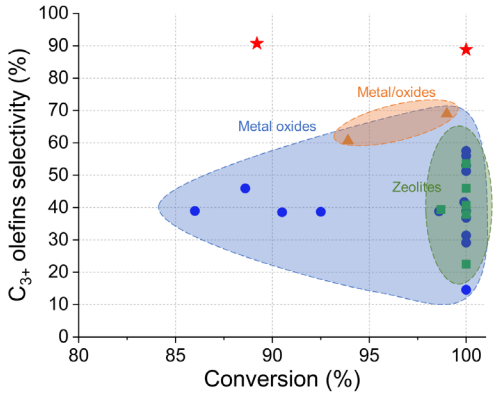

Figure 3. Ethanol conversion and C_{3+} olefin selectivity over different pathways and different catalyst types. Blue region: pathway with acetone intermediate over metal oxides; Green region: pathway with ethylene intermediate over Brønsted acid zeolites; Orange region: pathway with butadiene intermediate over transition metal modified oxides; Red star: this work. Detailed information on catalysts, and reaction conditions is reported in Table S1.

catalyst is likely not as sensitive to water as other base catalysts, such as HAP or MgO[30].

The C_{3+} olefin selectivity and olefin composition are critical for the downstream oligomerization reaction, liquid hydrocarbon yield and fuel quality. Figure 3 shows the C_{3+} olefin selectivity as a function of ethanol conversion to represent the potential of each route for direct ethanol conversion to C_{3+} olefins. The Lewis acid zeolite catalyzed C-C bond formation pathway (via acetaldehyde) identified in this study exhibits significantly higher C_{3+} olefin selectivity, in comparison with other direct ETO approaches, namely, Brønsted acid zeolite catalyzed C-C bond formation via ethylene[31], oxide material catalyzed pathway via the acetone intermediate[16,32], transition metal modified oxides with butadiene as the intermediate[13]. Cu-Zn-Y/Beta catalyst offers a unique active site combination to promote high selectivity of C_{3+} olefins by minimizing ethanol dehydration to ethylene and avoiding significant C-C cleavage and over hydrogenation of olefins, which lead to CO_2 and light paraffins formation, respectively.

Beyond the C_{3+} olefin selectivity consideration, olefin composition is also critical since different olefins have distinct reactivities in the oligomerization reaction, for example, butenes are more favored than other olefins[17,20], such as propene and C_{5+} olefins, so it is desired to produce olefins with higher concentrations of butenes. Cu-Zn-Y/Beta catalyst is able to produce C_{3+} olefins with 75% butenes, which is much higher than that from Brønsted acid zeolite catalyzed pathway and oxide-based pathway over the majority of oxide catalysts (Table S1). Furthermore, this pathway can be operated at much lower reaction temperatures (623 K or lower) than all the other direct ETO pathways (673-823 K) (Table S1). Such low-temperature operation can facilitate the integration with the downstream oligomerization reaction by significantly reducing the need of heat exchanging and potentially lowering the operation cost.

2.1.3. Flexible co-production of butadiene by modulating the hydrogen partial pressure. As shown in Scheme 1, there are two competitive pathways of converting crotonaldehyde i.e., hydrogenating C=C over Cu sites in the presence of hydrogen or reducing C=O via MPV reduction. Hydrogen could play an important role in affecting the relative rates of these two reactions, thus leading to different product distributions. We investigated the impact of hydrogen partial pressure on ethanol conversion and product selectivities (Figure 4, Figure S3).

The major impact of hydrogen partial pressure is on the selectivities of butadiene, butenes and C_{3+} olefins. Reducing hydrogen partial pressure is likely to slow down the hydrogenation steps (steps 3 and 8, Scheme 1) as hydrogen partial pressure generally has a positive impact on hydrogenation over Cu sites[33,34]. When no hydrogen was co-fed,

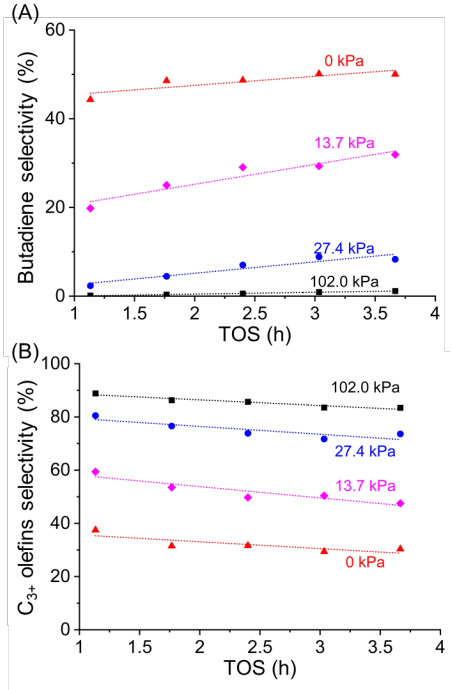

Figure 4. Selectivities of (A) butadiene and (B) C_{3+} olefins at different hydrogen partial pressures. Reaction conditions: 623 K, 0.53 h^{-1} WHSV, total pressure 109.6 kPa, 7.6 kPa ethanol balanced with He. Conversion and other products selectivities are reported in Figure S3.

butadiene selectivity is approaching 50% (Figure 4) while the amount of butenes is only ~14% (Figure S3), suggesting crotonaldehyde is primarily converted to butadiene via crotyl alcohol in the absence of hydrogen. This is consistent with conventional ethanol to butadiene reaction, where crotyl alcohol is proposed to be the major intermediate to butadiene[35] and the hydrogenation of crotonaldehyde to crotyl alcohol is via MPV reaction. We would like to note that there are still significant opportunities to optimize the butadiene selectivity via catalyst and reaction optimizations; however, the primary goal of this study is to demonstrate the flexible co-production of butadiene along with significant C_{3+} olefins formation for synthesizing liquid hydrocarbon fuels. As we increase the hydrogen partial pressure to 13.7 kPa and 27.4 kPa, butadiene

selectivity decreases to 20% and 2.3% at 1.1 h TOS, respectively, along with a dramatic increase of butene selectivity to 40% and 60%. When cofeeding 102.0 kPa hydrogen, butadiene formation is completely inhibited while butene selectivity reaches 62%. Interestingly, hydrogen partial pressure does not show a significant impact on total C_4 products (sum of butenes and butadiene) (Figure S3). The C_{3+} olefin selectivity is also varied between 37% and 89% at 1.1 h TOS as we increase the hydrogen partial pressure from 0 to 102.0 kPa (Figure 4). These findings indicate that the ratio between butadiene and C_{3+} olefins can be tuned by simply varying the amount of hydrogen cofeeding, so that we can adjust the ratio of final liquid hydrocarbon fuel yield and the coproduct.

2.1.4 Oligomerization of C_{3+} olefins. The C_{3+} olefins obtained from ETO were further oligomerized to longer-chain hydrocarbons over several solid acid catalysts, including Amberlyst-15, Amberlyst-36, and CT275. Figure 5A shows the liquid hydrocarbon distributions in gasoline, jet and diesel cuts based on the simulated distillation of the oligomerization liquid products (Figure S4). Over Amberlyst-36, 80 wt.% of middle distillate (47% jet and 33% diesel) is obtained with 15% gasoline fraction and a minor heavy fraction (3%, >663 K). Amberlyst-15 is shown to generate a higher fraction of longer-chain hydrocarbons as reflected by 91 wt.% combined middle distillate and heavy fractions and less gasoline fraction in comparison with Amberlyst-36. On the other hand, CT275 tends to produce higher gasoline fraction (25 wt.%) than Amberlyst-36 (15 wt.%) and Amberlyst-15 (9.0 wt.%). These findings suggest the gasoline, jet and diesel cuts could be adjusted by working with different oligomerization catalysts. Over all these catalysts, iso-paraffins and olefins are the primary types of hydrocarbons along with small amounts of n-paraffins (or olefins), naphthenes and aromatics (Figure 5B). Further optimization of the middle distillate yield and adjusting the composition is possible with other oligomerization catalysts (e.g., zeolites[19,36]), which is out of the scope for this investigation since olefin oligomerization has been a topic of prior extensive studies[19,36]. The carbon conversion efficiency for the overall ethanol to hydrocarbon process is shown in Table S2. The process described in this study shows high carbon efficiencies from ethanol to liquid hydrocarbons and middle distillates (85% and 74%, respectively).

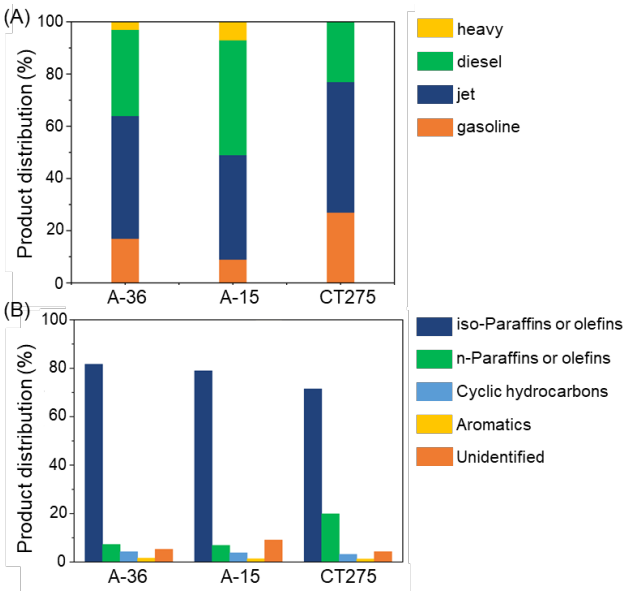

Figure 5. Liquid hydrocarbon distributions after oligomerization over Amberlyst-36 (A-36, 423 K, 54 bar), Amberlyst-15 (A-15, 423 K, 40 bar) and CT275 (393 K, 39 bar). (A) Gasoline cut (initial boiling point to 426 K), jet cut (426-529 K), diesel cut (529-663 K), and heavy cut (>663 K). (B) Types of hydrocarbons in the liquid products.

2.2 TEA and process design

2.2.1 Ethanol upgrading costs and sensitivity analysis. The process described in this TEA model (n^{th}-plant analysis) includes feedstock handling, pretreatment, saccharification (or enzymatic hydrolysis), fermentation, distillation and product recovery for ethanol, and ethanol upgrading to hydrocarbon fuels and butadiene (Scheme S1). Ethanol upgrading cost is calculated by considering capital expense (CAPEX) and operation cost (including fixed operating cost, catalyst, hydrogen and utilities) for the downstream catalytic conversion processes, comprising ETO, oligomerization, hydrotreating and associated separations, where the modeling of ETO and oligomerization steps is based on the experimental inputs (section 2.1) while the hydrotreating step and separations are based on a prior model[2]. The base case starts with nearly pure anhydrous ethanol for the ETO reactor without considering coproducts and the process parameters are summarized in Table S3. The baseline ethanol upgrading cost with pure ethanol feed is \$0.60/GGE (gasoline gallon equivalent), where the CAPEX contributes 27% of the overall upgrading cost (\$0.16/GGE), while OPEX makes up the other 73% (Figure 6). The hydrotreating reactor cost contributes to 49% of the overall CAPEX, followed by ETO reactor and oligomerization reactor (Figure S5). In comparison with ethanol to jet (ETJ) based on the two-step ethanol to butene-rich olefins shown in Tao et al.[37], the one-step ETO shows ~42% reduction in ethanol upgrading cost (\$0.60/GGE vs \$1.04/GGE).

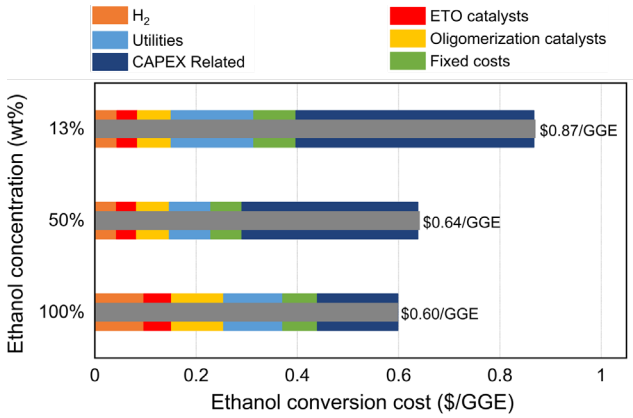

Figure 6. Ethanol upgrading cost distributions for three cases with different ethanol concentrations.

A single-point sensitivity analysis was performed to understand the impact of process parameters on ethanol upgrading cost as illustrated in the tornado chart (Figure 7). The variables with the most significant impact on cost would show on the top of the tornado chart. Among these selected variables and their ranges, CAPEX, ETO reactor inlet ethanol concentration, liquid hydrocarbon yield, and WHSV for both oligomerization and ETO show significant impact on the ethanol upgrading cost.

For ETO reactor inlet ethanol concentration, besides the anhydrous ethanol case, two additional scenarios of ethanol feeds with different ethanol concentrations were considered for this ethanol-to-middle-distillate process concept, including 13% (wt.%) and 50% ethanol, which represent the ethanol concentrations in the effluent streams from fermentation and beer column distillation, respectively (Scheme S1). For the 13% ethanol scenario, the additional cost for removing impurities from the fermentation broth was not considered, so it represents the minimum cost to work with such ethanol concentration. The main purpose is to understand the impact of water content on the overall cost to select the most practical separation strategy prior to ethanol catalytic upgrading. As we vary the ETO reactor inlet ethanol concentration from 100% to 13%, the conversion cost increases from \$0.60 to \$0.87/GGE (45% increase, Figure 6 and 7), mainly due to the increase of ETO reactor size and heat demand due to the introduction of extra amount of water into the ETO reactor. An optimum MFSP (with corn starch ethanol feed as an example) is reached at the medium ethanol content (Table S4), where \$0.11/GGE could be saved in comparison with the pure ethanol scenario. Aqueous ethanol feed with partial purification is also preferred in another study on a different consolidated alcohol dehydration and oligomerization approach by Hannon et al[8]. Experimentally this is feasible since cofeeding a certain amount of water does not affect the catalyst performance, at least up to the time on stream evaluated within this study (Figure S2). This increases the flexibility of this biorefinery concept as ethanol production is often accompanied by water.

The C_{3+} olefin selectivity is directly related to the liquid hydrocarbon yield, one of the key cost drivers as shown in Figure 7. The modeled yield for our base case is 0.58 GGE/gallon ethanol based on our experimental inputs with ~89% C_{3+} olefin selectivity and 100% ethanol conversion (623 K). A decrease of the liquid hydrocarbon yield to 0.43 GGE/gallon ethanol (corresponding to ~66% C_{3+} olefin selectivity, which still exceeds the majority of one-step ETO pathways reported in the literature as shown in Figure 3 and Table S1) would lead to a significant increase of the conversion cost by 37% (\$0.22/GGE, Figure 7). This highlights the importance of obtaining high selectivity to C_{3+} olefins and demonstrates the advantage of this one-step ETO approach when compared with other existing ethanol conversion methods (Figure 3). Meanwhile it also indicates the significance of further improving the C_{3+} olefin selectivity through experimental R&D, which could be achieved via catalyst or reaction optimization, such as modifying the catalyst acidity or lowering the reaction temperature to inhibit ethylene formation (Figure 2).

WHSVs for both oligomerization and ETO steps are critical to ethanol upgrading cost as illustrated in Figure 7. Increasing the active site densities or replacing them with more active metal centers for both aldol condensation and hydrogenation are potential strategies for promoting the catalyst activities. For instance, ethanol conversion decreases to 59% with the increase of acetaldehyde and butadiene selectivity to 21% and 15%, respectively, when the WHSV is increased to 2.9 h^{-1} (residence time 0.34 g_{cat} h g_{EtOH}^{-1} as shown in Figure S1). Further improvement of the aldol condensation (reaction step 2, Scheme 1) and hydrogenation activities (reaction steps 3, 4, 6 and 9, Scheme 1) would favor the formation of butenes.

CAPEX is also affecting ethanol upgrading cost significantly as shown in Figure 7 and there are potential opportunities to reduce capital expense per GGE. One scenario is through increasing the biorefinery size. The annual ethanol production in the current analysis is 39 million gallons. Increasing the biorefinery size could lead to a decrease of capital cost/GGE and MFSP due to economy of scales[38]. Another opportunity is to save cost over the hydrotreating step, where the hydrotreater is the largest cost component among all the downstream upgrading and separation units (49% of the total installed equipment capital cost, Figure S5). One potential scenario is

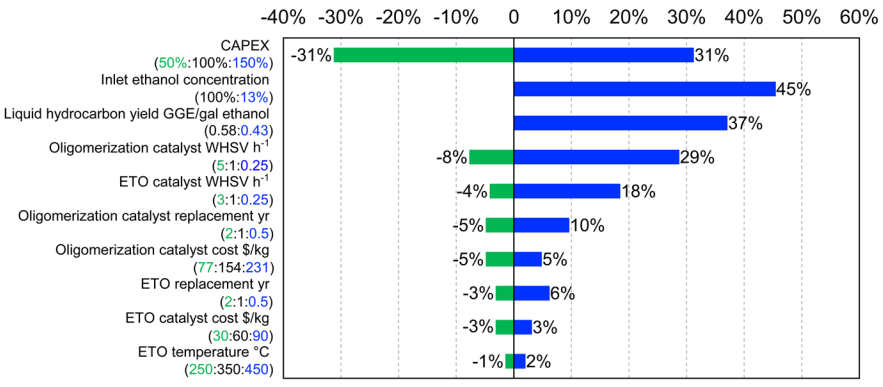

Figure 7. Sensitivity analysis of major ethanol upgrading process parameters.

that the liquid hydrocarbons collected after the oligomerization step can be transported to a central refinery for further hydrotreating and blending with other hydrocarbon streams to make jet/diesel fuel, where the size of the hydrotreater in the central refinery could be dramatically larger than the one used in the biorefinery modeled here. Utilization of hydrotreating facilities in the existing petroleum refineries via a co-processing scheme offers another option to reduce the MFSP further. Similar types of concepts have been applied in biomass hydrothermal liquefaction[39], where significant cost benefit could be obtained either via a central refinery concept or using a co-processing scheme with petroleum refinery streams. In summary, the sensitivity analysis has indicated opportunities to reduce the ethanol upgrading cost via further catalyst development to improve C_{3+} olefin selectivity and WHSV, process optimization on balancing dewatering of ethanol feed prior to catalytic upgrading steps and a new process scheme of processing oligomerization liquid products in either a larger central hydrotreating facility or coprocessing with petroleum feed.

2.2.2 MFSP based on different ethanol feedstocks. This ethanol-to-middle-distillate process can be used as a bolt-on technology with an ethanol biorefinery to produce various hydrocarbon fuels and chemical coproducts to expand the product portfolios from ethanol. To understand the cost of making liquid hydrocarbon fuels, MFSPs were calculated by adding up the ethanol price and ethanol upgrading cost (see calculation details in section 4.3). Both first-generation (corn starch) and second-generation ethanol (corn stover) were considered and three cases were evaluated for each of the feedstocks, including current case, projected case and BD coproduction case (Table 2). The current cases are based on current ethanol fermentation technologies and the baseline ethanol upgrading cost in this study ($0.60/GGE), where the 2010-2020 10-year average corn starch ethanol price and cellulosic ethanol price reported in NREL 2011 design model[40] were used. For the projected cases, lower ethanol prices were considered, 2015-2020 5-year average ethanol price for corn starch and projected cellulosic ethanol price for corn stover[8]. Projected ethanol upgrading technology with the improvement of liquid hydrocarbon yield to 95% of the theoretical maximum was considered in the projected cases. For the BD coproduction cases, 44% carbon from ethanol went to butadiene while the remaining carbons were sent for fuel production. The average and high U.S. Gulf Coast Kerosene-Type spot price of petroleum jet fuel in 2010-2020 ($2.00/GGE and $2.97/GGE, respectively)[41] were used as benchmarks to understand the competitiveness of ethanol derived liquid hydrocarbon fuels.

MFSPs of the current case based on corn starch and corn stover are higher than the petroleum jet fuel prices due to high ethanol prices. Since ethanol price is the dominant contributor to MFSP, maximizing the carbon conversion efficiency (particularly optimizing C_{3+} olefin yield) to increase liquid hydrocarbon yield is critical to lower the MFSP. As shown in Figure S7, further increase of the liquid hydrocarbon yield could dramatically lower the MFSP, e.g., $0.24/GGE cost reduction can be achieved by increasing the liquid hydrocarbon yield to 95% of the theoretical maximum. With lower ethanol prices and improved ethanol upgrading technology (95% of the theoretical maximum liquid hydrocarbon yield), the projected MFSPs are expected to drop down to $2.78/GGE and $2.80/GGE with corn starch and corn stover, respectively (Table 2), in a range that is comparable with the petroleum jet fuel prices.

Further cost reduction is considered with butadiene as a chemical coproduct, which can be produced by modulating the hydrogen partial pressure (as shown in section 2.1.3) and the remaining mono-olefin stream can be further oligomerized to

Table 2. MFSPs based on different feedstocks within three different scenarios

Feedstock	Case	Ethanol Prices ($/gal)	Ethanol upgrading technology	Upgrading Costs ($/GGE)	MFSP ($/GGE)	Average jet fuel price ($/GGE)[1]	High jet fuel price ($/GGE)[1]
Petroleum	Benchmark					$2.00	$2.97
Corn starch	Current	$1.80[2]	Baseline	$0.60	$3.70		
	Projected	$1.41[3]	Projected[4]	$0.53	$2.78		
	BD coproduction[5]	$1.41	BD coproduction	----	$1.64		
Corn stover	Current	$2.54[6]	Baseline	$0.60	$4.98		
	Projected	$1.42[7]	Projected	$0.53	$2.80		
	BD coproduction[5]	$1.42	BD coproduction	----	$1.70		

[1] Average and high U.S. Gulf Coast Kerosene-Type spot price of petroleum jet fuel in 2010-2020[41]. [2]2010-2020 10-year average corn ethanol price is used. The historical ethanol selling price is shown in Figure S6. [3]2015-2020 5-year average corn ethanol price is used. [4]The projected ethanol upgrading technology assumes 95% of the theoretical maximum liquid hydrocarbon yield. [5]BD coproduction case considers 44% carbon from ethanol goes to butadiene with butadiene selling price of $0.8/lb. [6]Ethanol selling price for current case with corn stover is calculated from NREL 2011 model[40] after adjusting the cost to 2016$. [7]Ethanol selling price for the projected case with corn stover is based on future cellulosic ethanol technology updated to 2016$[8].

make liquid hydrocarbons. Figure 8 shows the MFSP changes as a function of butadiene price and ethanol price. At fixed ethanol price, increasing butadiene price would reduce the MFSP with coproduct credit. At the ethanol price of $1.41/gallon (2015-2020 5-year average price for corn starch ethanol), a minimum BD selling price of $0.59/lb is needed to achieve the same MFSP as the no coproduct case (corn starch-projected case). Any BD price above $0.59/lb would lead to further MFSP reduction, for example, MFSP drops to $1.64/GGE with a butadiene price of $0.80/lb (2010-2015 average BD price as shown in Figure S8), making corn ethanol derived hydrocarbon fuel competitive with the petroleum benchmark. With corn stover as the feedstock, the MFSP can be lowered to $1.70/GGE when producing butadiene ($0.80/lb) as the coproduct (Table 2), also in the similar range as petroleum-derived jet fuel. Since butadiene price fluctuated largely (Figure S8), coproduction of butadiene can be adjusted based on the market price and demand accordingly by leveraging the flexible operation of the ETO step.

Altogether, we have shown that lower ethanol prices and improvement of liquid hydrocarbon yield lead to significant MFSP reduction for both corn starch ethanol and corn stover ethanol. Coproduct credits from ethanol (e.g., butadiene) are critical to further bring down the cost to improve the long-term competitiveness. Beyond these opportunities, carbon credits due to the benefits of lower GHG emissions from these ethanol-derived fuels could potentially further enhance the cost competitiveness, so the life-cycle analysis was performed to evaluate the carbon intensities.

2.3 Life-cycle analysis

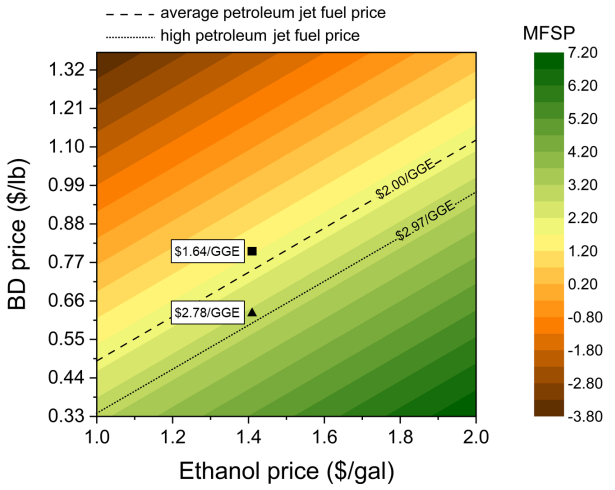

Figure 8. Contour plot of MFSP vs. ethanol price and BD price. The triangle represents the minimum BD price at ethanol prices of $1.41/gal, above which BD coproduction will help to reduce the MFSPs compared with no BD scenarios (projected cases). The square shows the BD coproduction case for corn starch. Average and high petroleum jet fuel prices are the average and high U.S. Gulf Coast Kerosene-Type spot price in 2010-2020, respectively[41].

Nine cases are selected to evaluate the Well-to-Wake (WTWa) analysis results under different scenarios such as the type of feedstock (corn starch, corn stover, and miscanthus), hydrocarbon yield (0.58 and 0.43 GGE/gal ethanol), and ethanol concentration (13%, 50%, and 100%) (Figure 9). Both Case 1 and 5 are based on the TEA current cases with corn starch and corn stover as feedstock, respectively. The additional cases were studied to understand the impact of feedstock, liquid hydrocarbon yield and ethanol concentration on GHG emissions.

The feedstock type affects the upstream GHG emissions, which includes farming/collection, fertilizer/pesticide use, transportation, and land-use change (LUC) impact. Greenhouse gases, Regulated Emissions, and Energy use in Technologies (GREET®) model was used for ethanol production from these three feedstocks[42]. The WTWa pathways of biomass-based and fossil-based jet fuel are shown in Figure S9. Since GREET assumes the production of 100% ethanol, the heat demand is adjusted for the cases of 13% and 50% ethanol to avoid double counting of energy requirements for ethanol purification. Major parameters and key assumptions of life cycle analysis of ethanol supply chain are presented in Table S5 and material inputs for ethanol purification and upgrading are shown in Table S6. Heat integration was considered between ethanol and jet fuel production to reduce the natural gas (NG) inputs. Since the liquid hydrocarbon fuel consists of gasoline, diesel, jet, and heavy oil, the energy-based allocation is assumed for the remaining fuel products other than jet fuel to obtain the LCA results for jet fuel.

Figure 9 shows the WTWa GHG emissions of jet fuel for nine cases along with the petroleum reference case. Cases 1 to 4 using corn starch ethanol have a large portion of GHG emissions from corn farming and ethanol fermentation. Since the ethanol purification represents the process of increasing the ethanol concentration to the target content, higher ethanol concentration is linked with more GHG emissions during purification. On the other hand, NG consumption in the downstream upgrading process decreases when the ETO reactor inlet ethanol concentration is high. Consequently, the NG saved by omitting the purification process is offset with the NG required for heating up the ETO inlet stream, so potentially an optimum case can be reached. Considering the net impact, Case 1 and 2 have lower carbon intensity (CI) than Case 3, indicating higher ethanol concentration for the ETO reactor inlet could benefit the overall GHG emission. Comparing Case 4 with Case 1, lower liquid hydrocarbon yield leads to significant increase of GHG emission to 90 gCO_2e/MJ due to the need of more ethanol feedstock and consuming more energy in the downstream ethanol upgrading process for producing the same quantity of jet fuel.

Due to lower CI of corn stover ethanol production compared to that of corn starch ethanol, Cases 5–8 present much lower GHG emissions mainly because of reduced GHG emissions from upstream biomass farming/collection, ethanol fermentation and purification compared to Cases 1–4. Corn stover-based ethanol plants use biomass instead of NG to provide heat for ethanol fermentation and purification. Since the combustion

emission of biomass is excluded from the LCA count, the GHG emissions of fermentation and purification are lower than those of corn starch cases. Among these cases, Cases 5 has low CI (13 gCO_2e/MJ), a ~85% reduction compared to the petroleum jet reference. Case 9 uses miscanthus as the feedstock for ethanol production, which presents a net GHG emission of -3.8 gCO_2e/MJ, ~105% lower than the reference, which is primarily due to using biomass to provide the process heat and the large negative LUC GHG emissions caused by its high crop yield[43].

WTWa GHG emissions from this study were compared with previous studies on ethanol-to-hydrocarbon technologies[37], where similar boundary conditions were selected for fair comparison. Han et al.[44] analyzed the ETJ technology via ethylene intermediate (two-step ethanol to butene-rich olefins) with jet fuel production integrated with biorefinery, using 100% ethanol from corn starch. CI of jet fuel from corn starch via this technology (72 gCO_2e/MJ) is 13% higher than Case 1 mainly due to higher energy consumption for the downstream ethanol conversion process. Altogether, the biomass feedstock type, liquid hydrocarbon yield and ethanol concentration for the ETO step are shown to impact the overall GHG emissions.

Carbon intensity reduction could lead to a significant economic incentive for producing renewable hydrocarbon fuels from ethanol. Based on California's Low Carbon Fuel Standard (LCFS), the carbon intensity reduction would provide credits of \$0.50/GGE and \$1.70/GGE to MFSPs with corn starch and corn stover as feedstocks (LCA case 1 and 5), respectively (Table S7). Renewable identification numbers (RINs) applied under the US Environmental Protection Agency (EPA) Renewable Fuel Standard (D3 for cellulosic feedstocks, and D6 for starch feedstocks) would provide further credits, \$0.02/GGE for corn starch and \$1.14/GGE for corn stover. With these carbon credits (e.g., biojet production in California), the MFSP for corn stover-derived liquid hydrocarbons (Table S7) will fall into the range comparable with the petroleum-based jet fuel prices.

2.4 Market flexibility

This conceptual biorefinery based on the ethanol platform shows several opportunities to be market responsive: 1) flexibility to take different alcohol feedstocks, such as wet ethanol with varied water content or alcohol mixture; 2) flexibility to produce different types of hydrocarbon fuel products; 3) the process could adjust the carbon flow to fuels and coproducts (e.g., butadiene) based on the market demand and price.

As discussed in section 2.1.2, water does not show a significant impact on catalyst performance, which offers the opportunity for directly using wet ethanol as feedstock for ethanol to middle distillate. Further, beyond ethanol, here we also show that the Cu-Zn-Y/Beta catalyst can directly convert a more complex mixture of acetone, 1-butanol and ethanol (ABE) to butene-rich C_{3+} olefins (95% selectivity at 99% total carbon conversion, Figure S10). The flexibility of taking different alcohol feedstocks greatly expands the application opportunities for such ethanol upgrading technology, such as biomass fermentation-derived alcohols, ethanol Guerbet reaction derived mixed alcohols[45] and CO_2 derived alcohols[6,46].

This process is able to produce a hydrocarbon blendstock that can be fractionated to different types of fuels over different oligomerization catalysts (Figure 5), although it is not the purpose here to demonstrate an exhaustive list of

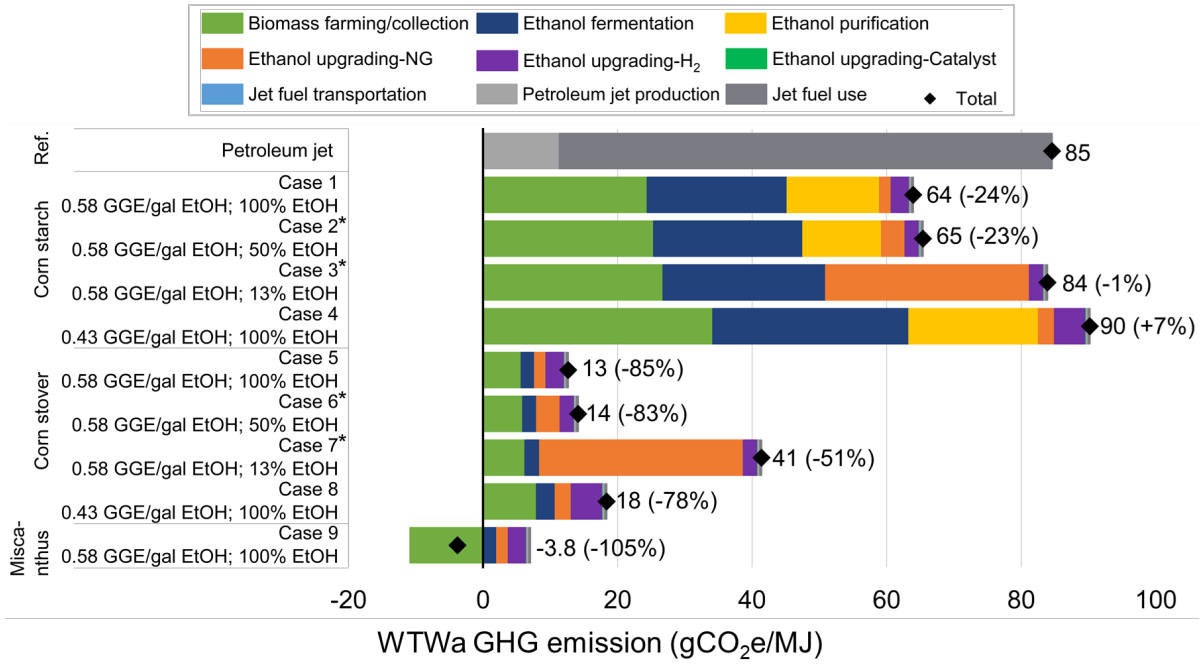

Figure 9. Well-to-Wake GHG emissions (gCO_2e/MJ jet fuel) of nine cases compared with the petroleum jet. GHG emissions from LUC are included in biomass farming/collection. CO_2 emissions from jet fuel use are offset by biogenic CO_2 in fuel for Cases 1-9. *For 50% and 13% ethanol concentration, slight carbon loss was observed in the downstream separation steps, which led to 3.4% and 8.6% decrease of liquid hydrocarbon yield, respectively. This difference is within the errors of both TEA and LCA calculations.

oligomerization catalysts and conditions in this study. This offers the flexibility to produce gasoline, jet and diesel, where when the market demand and price are favoring certain type of fuel, there is room to tune the process to meet the needs of the market changes without significant process modifications.

Coproduction of butadiene with hydrocarbon fuels from ethanol further enhances the process flexibility when the profit margin of butadiene is high enough. Figure S11 shows the amount of butadiene production when diverting different percentages of carbon from ethanol to butadiene and liquid hydrocarbon fuel, where we assume 10% of the predicted 2025 sustainable aviation fuel market (4.76 billion gallon/year[47]) is captured by ethanol to jet fuel. At high carbon conversion to butadiene (44%), the amount of butadiene produced from ethanol takes ~16% of predicted 2025 butadiene market, far below the market saturation point if we do not consider market penetration challenges of renewable butadiene. As the percentage of carbon to butadiene decreases to 30%, 20% and 10%, the market share of renewable butadiene from ethanol drops to 9.3%, 4.9% and 2.2%, respectively. This assessment indicates that butadiene is a promising coproduct for the ethanol-to-middle-distillate pathway to offset MFSP while potentially avoiding market saturation.

3. Conclusions

We report a market-responsive C_2 platform-based biorefinery concept for producing middle distillate fuels, which is enabled by our emerging ethanol upgrading technology based on one-step ethanol to butene-rich C_{3+} olefins. The development of Cu-Zn-Y/Beta catalyst enables the selective conversion of ethanol to C_{3+} olefins (89% selectivity at 100% ethanol conversion), greatly exceeding the olefin selectivities from all the other existing routes. TEA with experimental inputs has shown the ethanol upgrading cost is \$0.60/GGE, ~42% reduction in comparison with the ethylene-based ETJ approach. Key ethanol conversion cost drivers, such as liquid hydrocarbon yield, are identified to guide further R&D efforts. Coproduction of butadiene can help to significantly drive down the MFSP towards cost competitive with petroleum jet fuel based on either corn starch or corn stover ethanol. Life-cycle analysis has also indicated significant potential for GHG emission reduction, e.g., ~85% and ~105% GHG emission reduction with corn stover and miscanthus as feedstocks, respectively.

This study highlights the significance of developing one-step ETO in reducing the complexity of overall ethanol-to-middle-distillate process and lowering the ethanol upgrading cost. Further ETO catalyst development to increase the single-pass C_{3+} olefin yield and productivity, and optimize the olefin composition is critical for driving down the conversion cost and tuning fuel properties. This calls for in-depth understanding of the catalyst active sites and tuning the active sites (type or density) to minimize the side products (e.g., ethylene) and optimize the olefin compositions. The production of large-market-volume chemical coproducts is critical for increasing the cost competitiveness of the middle distillate fuels and enhancing the market responsiveness of the biorefinery. Moving forward, other coproduct opportunities could be explored in the context of ethanol to middle distillates, such as benzene, toluene and xylenes (BTX)[8], ethyl acetate, acetic acid, etc[48]. Environmental impact is another critical consideration, where other low-carbon-intensity feedstocks (such as CO_2) would potentially offer the opportunities to explore negative emission technologies for producing middle distillate fuels.

4. Experimental and methods

4.1 Catalyst synthesis

All the monometallic, bimetallic and trimetallic catalysts for ETO step were prepared by following similar procedure as reported in Zhang et al[11]. Briefly, the dealuminated Beta support was prepared by washing the parent zeolite Beta (from Zeolyst, SAR=12.5, CP814E) with nitric acid (Sigma Aldrich, 69% to 70%). Solid-state grinding approach was used to load the metal precursors (copper nitrate trihydrate (Sigma Aldrich, 98%), zinc nitrate hexahydrate (Sigma Aldrich, 97%) and yttrium nitrate hexahydrate (Sigma Aldrich, 97%)) onto DeAl-Beta. The sample was calcined at 823 K for 6 h with 1 K/min ramping rate under 16.7 $cm^3\ s^{-1}\ g_{cat}^{-1}$ air flow.

4.2 Catalyst characterization

Pyridine adsorption DRIFTS measurements were performed using a Cary 600 Series FTIR spectrophotometer equipped with a mercury-cadmium-telluride (MCT) detector, a Harrick Scientific Praying Mantis diffuse reflectance accessory, and an *in situ* chamber where the temperature and gas flow can be controlled. A hemispherical dome equipped with spectra-grade ZnSe windows from 4000-400 cm^{-1} with a 2 cm^{-1} resolution was used to collect the spectra (64 scans). All the samples were pretreated at 823 K with a rate of 5 K min^{-1} in 100 $cm^3\ min^{-1}$ 10% O_2 balanced with He (101.3 kPa total pressure) prior to cooling to 423 K. Samples were then saturated for 1800 s with gaseous pyridine carried in He using a bubbler setup, and then pure He was used to flush gaseous and physisorbed pyridine from the samples for 1800 s. Saturated spectra were then collected at 423 K followed by subtraction of the sample spectrum before pyridine adsorption to isolate peaks associated only with pyridine adsorption.

4.3 Ethanol conversion to C_{3+} olefins and olefin oligomerization

Ethanol conversion was carried out in a fixed-bed reactor as described in Cordon et al[10]. Typically, 0.15 g catalysts were pretreated by heating at 5 K min^{-1} to 673 K and held at 673 K under He flow (20 ccm) for 1 h to remove moisture before catalytic performance measurements. The flow rates of H_2 (Airgas, >99.999%), Ar (Airgas, >99.999%) and He (Airgas, >99.999%) were controlled with mass flow controllers. Pure ethanol (C_2H_5OH, >99%) was fed with a KD Scientific syringe pump followed by vaporizing inside the 1/8-inch stainless steel transfer lines heated to 423 K. An online gas chromatography (Agilent 7820A) equipped with both flame ionization detector (FID) and thermal conductivity detector (TCD) was applied to

analyze the products. The identification of products was analyzed with a gas chromatography (Agilent 6850) and mass spectrometer (Agilent 5975C). The carbon balance for ethanol conversion measurements was 92-96%.

The oligomerization experiments were performed in a high-pressure batch reactor (Parr Instrument) with similar operation procedure as shown in Adhikari et al[49]. Propylene (Airgas, 10% in nitrogen), 1-butene (Airgas, 99.5%), trans-2-butene (>99%), cis-2-butene (>99%), 2-pentene (Sigma Aldrich, mixture of cis and trans, 99%) and 2-hexene (Sigma Aldrich, mixture of cis and trans, 85%) were introduced into the batch reactor based on the olefin product compositions from ethanol conversion (2.34-3.91 g propene, 5.91 g 1-butene, 11.91 g trans-2-butene, 8.03 g cis-2-butene, 2.36 g 2-pentene and 4.46 g 2-hexene) with 10 g dried catalyst (Amberlyst-36 (Sigma Aldrich), Amberlyst-15 (Sigma Aldrich) and CT275 (Purolite)) and heated to operation temperatures and hold for 6 h and the products were analyzed with gas chromatography (Agilent 7820A) equipped with FID detector. Product identification was done by injecting samples into the gas chromatography (Agilent 6850) and mass spectrometer (Agilent 5975C). C_7-C_{40} hydrocarbon standards (Sigma Aldrich) were also used to help with product determination. Simulated distillation of the liquid hydrocarbons obtained from oligomerization was performed at Southwest Research Institute based on the ASTM D2887 test method.

4.3 TEA analysis

Process economics analysis was performed using a similar approach as described in Tao et al[37]. Briefly, the conceptual process design was developed with a detailed process flow diagram based on experimental data. Material and energy balance calculations were done via Aspen Plus. Capital and project cost estimations were carried out via an in-house model using spreadsheets.

The USDA corn grain dry mill model[50] is used as the front-end of the dry-mill-to-ethanol process at the scale of 1,037 dry ton per day. Since the ethanol production from corn grains have been commercialized for many years, we directly utilize the 2010-2020 historical ethanol selling price for our calculations of MFSP. For corn stover-based process, the base models are the NREL 2011 design models[40], with updates on financial assumptions such as 2016$ and feedstock cost of $84.45/dry ton. The scale is 2,000 dry ton per day.

Ethanol purification is redesigned to be suitable for ethanol upgrading. Literature data and assumptions are used to establish the fermentation yield basis[50,40]. Beer column distillation, rectification column distillation and molecular sieve dehydration are used to recover ethanol from the fermentation broth. Ethanol streams after the purification steps are further converted via ethanol to olefins, oligomerization, hydrotreating, and fractionations. For the first two upgrading steps, experimental reaction conditions and product distributions were used in the techno-economic analysis. The hydrotreating facility is used for the hydrotreating step based on 2013 NREL design report[51]. Final distillation columns are used to fractionate the hydrocarbon products from the light gases. Raw materials include ethanol, hydrogen, catalysts for both ETO and oligomerization, and utilities. Hydrogen is $0.7/lb, ETO catalyst is assumed to be $60/kg and oligomerization catalyst is assumed as $70/kg.

Based on published engineering methods[52], a discounted cash flow rate-of-return analysis was generated using capital and operating cost data, with financial assumptions consistent with previous studies[37]. The other assumptions include: 40% equity financing, 3 years of construction plus 6 months for startup, 30 years' plant life, 35% income tax and 5% of the fixed cost investment as the working capital. The MFSP ($/GGE) is the minimum price that the liquid fuel must sell for to generate a net present value of zero for a 10% internal rate of return (IRR). It is calculated as:

$$\mathrm{MFSP} = \left(\frac{\mathrm{MESP}}{Y} + \mathrm{EUC}\right) \times 100\% \quad (1)$$

Where MESP is the minimum ethanol selling price ($/GGE), Y is the liquid hydrocarbon yield (%) and EUC is ethanol upgrading cost ($/GGE). We would like to note that there are uncertainties around conceptual cost estimates. The cost values are best utilized in relative comparisons among technical variations or process improvements. It could be misleading to directly use the absolute values without understanding of the basis and assumptions. A single-point sensitivity analysis was performed using the variables related to the ethanol to olefins step and oligomerization step shown in Table S3. Reasonable minima and maxima for each variable were chosen to quantify the impact on ethanol conversion cost with all other factors held constant.

4.4 Life-cycle pathways and system boundaries.

We performed LCA using the GREET model developed by Argonne National Laboratory. Other GHGs (CH_4, N_2O, and uncombusted HCs) are included in the GHG emissions of jet fuel use. The WTWa results are presented in terms of gCO_2e/MJ (grams of CO_2 equivalent per MJ jet fuel) using the global warming potentials of 1, 30, and 265 for CO_2, CH_4, and N_2O, respectively. Since jet fuels are typically produced from petroleum refining, we consider the petroleum jet fuel production pathway as a reference case (WTWa of 84.6 gCO_2e/MJ). The system boundary of biomass-based jet consists of corn/miscanthus farming/collection, feedstock transportation, ethanol production and purification, jet production, jet transportation and distribution, and combustion. Ethanol from corn starch starts from corn farming, while ethanol from the corn stover starts from the collection stage because it is a byproduct. We only consider additional fertilizer/pesticide use for the corn stover[53]. Miscanthus-derived ethanol has the lowest upstream GHG emissions, mainly due to the negative LUC GHG emissions[43]. Corn ethanol plant uses natural gas to supply heat, whereas corn stover/miscanthus plants use biomass to supply heat. Produced jet from the ETJ process is transported/distributed through barge, pipeline, rail, and truck. At the end-use phase, the combustion CO_2 emissions from biomass-based fuel offset the

CO_2 absorbed during the biomass farming process, so we assumed carbon neutrality.

Conflicts of interest

United States patent application is pending for the inventor Z. L. B.H.D. is a co-inventor for a separate ethanol upgrading technology licensed to Vertimass, LLC.

Acknowledgements

J.Z., B.H.D. and Z.L. were sponsored by the U.S. Department of Energy, Office of Energy Efficiency and Renewable Energy (EERE), Bioenergy Technologies Office (BETO), under contract DE-AC05-00OR22725 (ORNL) with UT-Battle, LLC, and in collaboration with the Chemical Catalysis for Bioenergy (ChemCatBio) Consortium, a member of the Energy Materials Network. The work was also supported by the U.S. Department of Energy's Bioenergy Technologies Office under Contract No. DE-AC36-08GO28308 with the National Renewable Energy Laboratory. B.H.D. and Z.L. were also supported by the Center for Bioenergy Innovation, a DOE Bioenergy Research Center supported by the Office of Biological and Environmental Research in the DOE Office of Science and led by Oak Ridge National Laboratory. The views and opinions of the authors expressed herein do not necessarily state or reflect those of the United States Government or any agency thereof. Neither the United States Government nor any agency thereof, nor any of their employees, makes any warranty, expressed or implied, or assumes any legal liability or responsibility for the accuracy, completeness, or usefulness of any information, apparatus, product, or process disclosed, or represents that its use would not infringe privately owned rights. The authors acknowledge Dr. Todd Toops and Dr. Sreshtha Majumdar for experimental assistance with the DRIFTS analysis.

Notes and references

1 N. R. Baral, O. Kavvada, D. Mendez-Perez, A. Mukhopadhyay, T. S. Lee, B. A. Simmons and C. D. Scown, *Energy Environ. Sci.*, 2019, **12**, 807–824.

2 R. Davis, N. Grundl, L. Tao, M. Biddy, E. Tan, G. Beckham, D. Humbird, D. Thompson and M. Roni, *Process Design and Economics for the Conversion of Lignocellulosic Biomass to Hydrocarbon Fuels and Coproducts: 2018 Biochemical Design Case Update*, 2018.

3 A. Bailey, G. J. Leong and N. Fitzgerald, *Bioproducts to enable biofuels workshop summary report*, Office of Energy Efficiency and Renewable Energy (EERE), Washington, DC, 2015.

4 M. J. Biddy, C. Scarlata and C. Kinchin, *Chemicals from biomass: a market assessment of bioproducts with near-term potential*, National Renewable Energy Lab.(NREL), Golden, CO (United States), 2016.

5 Renewable Fuels Association, Annual Fuel Ethanol Production, ethanolrfa.org/statistics/annual-ethanol-production/, (accessed 13 November 2020).

6 F. Li, Y. C. Li, Z. Wang, J. Li, D.-H. Nam, Y. Lum, M. Luo, X. Wang, A. Ozden and S.-F. Hung, *Nat. Catal.*, 2020, **3**, 75–82.

7 C. K. Narula, Z. Li, E. M. Casbeer, R. A. Geiger, M. Moses-Debusk, M. Keller, M. V. Buchanan and B. H. Davison, *Sci. Rep.*, 2015, **5**, 16039.

8 J. R. Hannon, L. R. Lynd, O. Andrade, P. T. Benavides, G. T. Beckham, M. J. Biddy, N. Brown, M. F. Chagas, B. H. Davison, T. Foust and Z. Li, *Proc. Natl. Acad. Sci.*, 2020, **117**, 12576–12583.

9 L. Harmon, R. Hallen, M. Lilga, B. Heijstra, I. Palou-Rivera and R. Handler, *A Hybrid Catalytic Route to Fuels from Biomass Syngas*, LanzaTech, Inc., Skokie, IL (United States), 2017.

10 M. J. Cordon, J. Zhang, S. C. Purdy, E. C. Wegener, K. A. Unocic, L. F. Allard, M. Zhou, R. S. Assary, J. T. Miller, T. R. Krause, F. Lin, H. Wang, A. J. Kropf, C. Yang, D. Liu and Z. Li, *ACS Catal.*, 2021, **11**, 7193–7209.

11 J. Zhang, E. C. Wegener, N. R. Samad, J. W. Harris, K. A. Unocic, L. F. Allard, S. Purdy, S. Adhikari, M. J. Cordon, J. T. Miller, T. R. Krause, S. Cheng, D. Liu, M. Li, X. Jiang, Z. Wu and Z. Li, *ACS Catal.*, 2021, **11**, 9885–9897.

12 N. M. Eagan, M. D. Kumbhalkar, J. S. Buchanan, J. A. Dumesic and G. W. Huber, *Nat. Rev. Chem.*, 2019, 1.

13 V. L. Dagle, A. D. Winkelman, N. R. Jaegers, J. Saavedra-Lopez, J. Hu, M. H. Engelhard, S. E. Habas, S. A. Akhade, L. Kovarik and V.-A. Glezakou, *ACS Catal.*, 2020, **10**, 10602–10613.

14 Z. Li, A. W. Lepore, M. F. Salazar, G. S. Foo, B. H. Davison, Z. W. Wu and C. K. Narula, *Green Chem.*, 2017, **19**, 4344–4352.

15 W. Xia, F. Wang, X. Mu, K. Chen, A. Takahashi, I. Nakamura and T. Fujitani, *Catal. Commun.*, 2017, **73**, 27-33.

16 J. Sun, K. Zhu, F. Gao, C. Wang, J. Liu, C. H. F. Peden and Y. Wang, *J. Am. Chem. Soc.*, 2011, **133**, 11096–11099.

17 J. S. Lopez, R. A. Dagle, V. L. Dagle, C. Smith and K. O. Albrecht, *Catal. Sci. Technol.*, 2019, **9**, 1117–1131.

18 L. Lin, A. M. Sheveleva, I. da Silva, C. M. A. Parlett, Z. Tang, Y. Liu, M. Fan, X. Han, J. H. Carter and F. Tuna, *Nat. Mater.*, 2020, **19**, 86–93.

19 J. Q. Bond, D. M. Alonso, D. Wang, R. M. West and J. A. Dumesic, *Science*, 2010, **327**, 1110–1114.

20 D. M. McClean, Ph.D Thesis, University of Cape Town, 1987.

21 Prismane Consulting, Global Butadiene Market Overview, https://www.openpr.com/news/1831666/global-butadiene-market-overview, (accessed 12 December 2020).

22 P. C. A. Bruijnincx and B. M. Weckhuysen, *Angew. Chemie Int. Ed.*, 2013, **52**, 11980–11987.

23 J. Pang, M. Zheng, C. Wang, X. Yang, H. Liu, X. Liu, J. Sun, Y. Wang and T. Zhang, *ACS Catal.*, 2020, **10**, 13624–13629.

24 T. Yan, W. Dai, G. Wu, S. Lang, M. Hunger, N. Guan and L. Li, *ACS Catal.*, 2018, **8**, 2760–2773.

25 G. Pomalaza, P. A. Ponton, M. Capron and F. Dumeignil, *Catal. Sci. Technol.*, 2020, **10**, 4860–4911.

26 B. Saville, *Angew. Chemie Int. Ed. English*, 1967, **6**, 928–

939.
27 T. De Baerdemaeker, M. Feyen, U. Müller, B. Yilmaz, F. S. Xiao, W. Zhang, T. Yokoi, X. Bao, H. Gies and D. E. De Vos, *ACS Catal.*, 2015, **5**, 3393-3397.
28 V. Gutierrez, M. Dennehy, A. Diez and M. A. Volpe, *Appl. Catal. A Gen.*, 2012, **437**, 72–78.
29 C. Hammond, S. Conrad and I. Hermans, *Angew. Chemie Int. Ed.*, 2012, **51**, 11736–11739.
30 S. Hanspal, Z. D. Young, J. T. Prillaman and R. J. Davis, *J. Catal.*, 2017, **352**, 182–190.
31 J. Bi, M. Liu, C. Song, X. Wang and X. Guo, *Appl. Catal. B Environ.*, 2011, **107**, 68–76.
32 F. Hayashi and M. Iwamoto, *ACS Catal.*, 2013, **3**, 14–17.
33 A. Dandekar, R. T. K. Baker and M. A. Vannice, *J. Catal.*, 1999, **184**, 421–439.
34 R. A. Koeppel, J. T. Wehrli, M. S. Wainwright, D. L. Trimma and N. W. Cant, *Appl. Catal. A Gen.*, 1994, **120**, 163–177.
35 E. D. M. J. W. D. J. J. P. S. B. Makshina, *Chem. Soc. Rev.*, 2014, **43**, 7917–7953.
36 O. Muraza, *Ind. Eng. Chem. Res.*, 2015, **54**, 781–789.
37 L. Tao, J. N. Markham, Z. Haq and M. J. Biddy, *Green Chem.*, 2017, **19**, 1082–1101.
38 Y. Zhang, A. H. Sahir, E. C. D. Tan, M. S. Talmadge, R. Davis, M. J. Biddy and L. Tao, *Green Chem.*, 2018, **20**, 5358–5373.
39 L. J. Snowden-Swan, Y. Zhu, S. B. Jones, D. C. Elliott, A. J. Schmidt, R. T. Hallen, J. M. Billing, T. R. Hart, S. P. Fox and G. D. Maupin, *Hydrothermal Liquefaction and Upgrading of Municipal Wastewater Treatment Plant Sludge: A Preliminary Techno-Economic Analysis, Rev. 1*, Pacific Northwest National Lab.(PNNL), Richland, WA (United States), 2016.
40 D. Humbird, R. Davis, L. Tao, C. Kinchin, D. Hsu, A. Aden, P. Schoen, J. Lukas, B. Olthof and M. Worley, *Process design and economics for biochemical conversion of lignocellulosic biomass to ethanol: dilute-acid pretreatment and enzymatic hydrolysis of corn stover*, National Renewable Energy Lab.(NREL), Golden, CO (United States), 2011.
41 EIA, Weekly U.S. Gulf Coast Kerosene-Type Jet Fuel Spot Price FOB (Dollars per Gallon), https://www.eia.gov/dnav/pet/hist/LeafHandler.ashx?n=PET&s=EER_EPJK_PF4_RGC_DPG&f=W, (accessed 20 May 2021).
42 M. Wang, A. Elgowainy, U. Lee, A. Bafana, P. T. Benavides, A. Burnham, H. Cai, Q. Dai, U. Gracida, T. R. Hawkins, P. V. Jaquez, J. C. Kelly, H. Kwon, X. Liu, Z. Lu, L. Ou, P. Sun, O. Winjobi, H. Xu, E. Yoo, G. G. Zaimes and G. Zang, Greenhouse gases, Regulated Emissions, and Energy use in Technologies Model (2020), Argonne National Laboratory, Lemont, IL, 2020.
43 J. B. Dunn, S. Mueller, H. Kwon and M. Q. Wang, *Biotechnol. Biofuels*, 2013, **6**, 1–13.
44 J. Han, L. Tao and M. Wang, *Biotechnol. Biofuels*, 2017, **10**, 1–15.
45 K. K. Ramasamy, M. Gray, H. Job, D. Santosa, X. Shari, L. Arun, D. Abhi and K. Yong, *Top. Catal.*, 2016, **59**, 46–54.
46 Y. Pang, J. Li, Z. Wang, C.-S. Tan, P.-L. Hsieh, T.-T. Zhuang, Z.-Q. Liang, C. Zou, X. Wang and P. De Luna, *Nat. Catal.*, 2019, **2**, 251–258.
47 International Energy Agency, Aviation fuel consumption in the Sustainable Development Scenario, 2025-2040, https://www.iea.org/data-and-statistics/charts/aviation-fuel-consumption-in-the-sustainable-development-scenario-2025-2040, (accessed 7 January 2021).
48 J. Sun and Y. Wang, *ACS Catal.*, 2014, 4, 1078–1090.
49 S. P. Adhikari, J. Zhang, Q. Guo, K. A. Unocic, L. Tao and Z. Li, *Sustain. Energy Fuels*, 2020, **4**, 3904–3914.
50 J. R. Kwiatkowski, A. J. McAloon, F. Taylor and D. B. Johnston, *Ind. Crops Prod.*, 2006, **23**, 288–296.
51 R. Davis, L. Tao, E. C. D. Tan, M. J. Biddy, G. T. Beckham, C. Scarlata, J. Jacobson, K. Cafferty, J. Ross and J. Lukas, *Process design and economics for the conversion of lignocellulosic biomass to hydrocarbons: dilute-acid and enzymatic deconstruction of biomass to sugars and biological conversion of sugars to hydrocarbons*, National Renewable Energy Lab.(NREL), Golden, CO (United States), 2013.
52 M. Peters and K. Timmerhaus, *Plant Design and Economics for Chemical Engineers*, McGraw-Hill, Fourth Edi., 1991.
53 C. E. Canter, J. B. Dunn, J. Han, Z. Wang and M. Wang, *BioEnergy Res.*, 2016, **9**, 77–87.